World Journal of Mechanics, 2026, 16(9), 119-130
https://www.scirp.org/journal/wjm
ISSN Online: 2160-0503
ISSN Print: 2160-049X

Numerical Elucidation of Flow Characteristics Induced by Axial Clearance in a Rotating Disk

Hiroyuki Furukawa, Yusuke Nakatani

Department of Mechanical Engineering, Meijo University, Nagoya, Japan
Email: furukawa@meijo-u.ac.jp

How to cite this paper: Furukawa, H. and Nakatani, Y. (2026) Numerical Elucidation of Flow Characteristics Induced by Axial Clearance in a Rotating Disk. *World Journal of Mechanics*, **16**, 119-130.
https://doi.org/10.4236/wjm.2026.169007

Received: August 15, 2026
Accepted: September 13, 2026
Published: September 16, 2026

Abstract

Rotating disks play a critical role in various engineering applications, including turbines, water wheels, and hard disk drives. Despite their importance, the influence of disk geometry—particularly axial gaps—on flow behavior has not been sufficiently explored. This study conducts numerical simulations to investigate vortex structures generated around a rotating disk with varying axial gaps. Flow fields are analyzed using the second invariant of the velocity gradient tensor (Q-criterion), and vortex transitions are examined across Reynolds numbers ranging from 2500 to 20000. Results show that smaller axial gaps promote laminar-like vortex behavior, while higher Reynolds numbers induce transitions toward spiral vortex structures. The findings provide insight into flow mechanisms influenced by disk geometry and contribute to improved understanding of rotating disk systems.

Keywords

Rotating Disk, Axial Clearance, Vortex Structure, CFD

1. Introduction

Rotating disks are indispensable components in modern engineering systems, including turbines, water wheels, and hard disk drives (HDDs). Their flow characteristics have long served as canonical models for studying boundary-layer development, instability, and transition to turbulence. The historical foundation of rotating-disk research was established by von Kármán [1], who derived the classical self-similar solutions for rotating-disk boundary layers. This work was later extended by Bödewadt [2], who analyzed the counter-rotating flow formed above a stationary wall, laying the groundwork for rotor-stator cavity studies.

Building on these classical foundations, numerous experimental and numerical investigations have revealed the rich instability mechanisms inherent in rotating-disk systems. Schouveiler *et al.* [3] demonstrated that confined rotor-stator flows exhibit spiral waves, circular waves, and complex transitional patterns that depend strongly on Reynolds number and cavity geometry. More recently, Alfredsson and Lingwood [4] provided a modern review of rotating-disk and rotating-cone flows, highlighting cross-flow instabilities and absolute instabilities as key mechanisms governing transition. High-order large-eddy simulations by Viaszzo *et al.* [5] further clarified the three-dimensional vortex structures that arise in confined rotor-stator cavities, emphasizing the sensitivity of vortex morphology to geometric confinement.

Within the broader context of rotor-stator research, several studies have examined how cavity geometry influences instability and vortex formation. Launder *et al.* [6] reviewed laminar, transitional, and turbulent flows in rotor-stator cavities, emphasizing the dominant role of confinement in determining vortex behavior. Lopez *et al.* [7] showed that spiral vortices in Bödewadt-type flows originate from cross-flow instabilities that are highly sensitive to axial spacing. Cros and Le Gal [8] reported spatiotemporal intermittency in torsional Couette flow between rotating and stationary disks, demonstrating that axial confinement strongly affects vortex organization. Spohn *et al.* [9] further revealed that vortex breakdown in confined rotating-disk flows is closely linked to the axial gap and the resulting pressure distribution.

Despite these extensive studies, the influence of axial clearance—the vertical gap between the rotating disk and the confining boundaries—has not been systematically investigated. Most prior work has focused on global aspect ratios or cavity-scale confinement, rather than localized axial gaps directly adjacent to the rotating disk. The present study addresses this gap by numerically analyzing vortex structures generated around a rotating disk with systematically varied axial clearance. Using the second invariant of the velocity gradient tensor (Q-criterion), vortex transitions are examined across Reynolds numbers ranging from 2500 to 20000. The objective is to elucidate how axial confinement governs the transition from bead vortices to sickle vortices and ultimately to spiral vortices, thereby positioning axial-gap effects within the broader framework of rotating-disk and rotor-stator flow research.

2. Numerical Model

2.1. Experimental Apparatus Model

Figure 1 is a schematic diagram of the experimental apparatus to be analyzed. The numerical model replicates a cylindrical container designed to investigate flow structures generated by a rotating disk. The container consists of two stationary disks positioned at the top and bottom, forming the axial boundaries of the domain. A cylindrical frame with a radius of 142.0 mm and a thickness of 40.0 mm encloses the system. The rotating shaft and the disk-mounting section have a diameter of 20 mm, ensuring structural consistency with typical mechanical configurations.

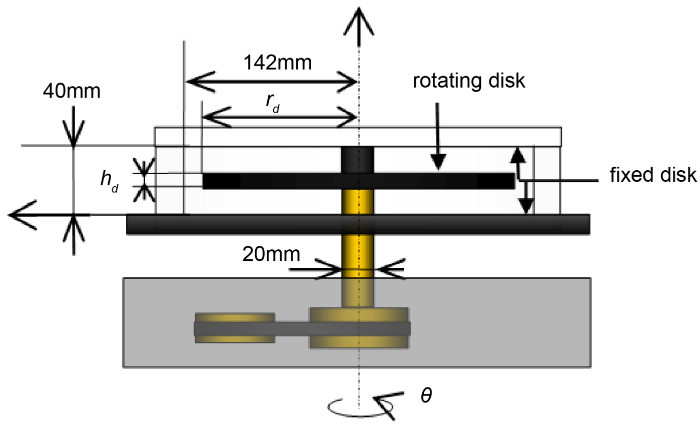

Figure 1. Analysis target.

The interior of the container is entirely filled with the working fluid, allowing the simulation to capture the interaction between the rotating disk and the confined fluid environment.

2.2. Rotating Disk Geometry

The rotating disk, positioned centrally within the cylindrical container, is modeled with the following dimensions:

- Disk radius: $r_d = 127.0$ mm
- Disk thickness: $h_d = 10.0, 20.0, 30.0$ mm

These thickness variations directly modify the axial gap between the rotating disk and the stationary upper and lower disks. By systematically altering h_d, the study isolates how axial confinement influences vortex formation, flow transitions, and velocity distributions.

3. Computational Conditions

3.1. Numerical Method

The governing equations are the 3-dimensional incompressible Navier-Stokes equations and the equation of continuity. The equations are differentiated by the finite differential method. The computational domain was discretized using a structured mesh tailored to the cylindrical geometry of the container. A total of 265 radial, 338 circumferential, and 81 axial grid points were employed, yielding 7,255,170 cells in the full domain. This resolution was selected to ensure adequate spatial fidelity for capturing the steep velocity gradients and vortex structures that develop within the narrow axial and radial gaps surrounding the rotating disk. As the initial condition, all velocity components are zero in the entire domain. The boundary conditions of the walls are non-slip conditions for the velocity components, and Neumann conditions for the pressure.

We confirmed that the vortex components and Q-distribution changed by less than 2% between the medium and fine meshes, and that the residual and time interval are sufficiently small.

3.2. Definition of Reynolds Number

The Reynolds number for the rotating disk is defined as:

$$Re = \frac{UL}{\nu} \tag{1}$$

where U represents the characteristic velocity, L the characteristic length scale, and ν the kinematic viscosity of the working fluid. For a rotating disk, the circumferential velocity at the disk surface is used as U, and the disk radius r_d serves as L.

Simulations were conducted for Reynolds numbers ranging from 2,500 to 20,000, in increments of 2,500. This range allows systematic observation of flow transitions from laminar vortex structures to transitional and turbulent regimes.

3.3. Time Step and Simulation Duration

A uniform time step of 0.001 s was applied across all simulation cases. Each computation was advanced to 100 s, ensuring that transient behaviors had sufficiently decayed and that the vortex structures were fully developed prior to visualization and analysis.

4. Vortex Structure Theory

In general, as the Reynolds number increases, the vortex flow over a rotating disk transitions in the order shown in Figure 2: (a), (b), and (c). In case (a), bead-shaped vortices (bead vortices) appear in the radial gap. These bead vortices collapse and merge with one another, forming the sickle-shaped vortices shown in (b). As the flow further transitions toward the turbulent regime, spiral vortices appear in the axial gap, as shown in (c).

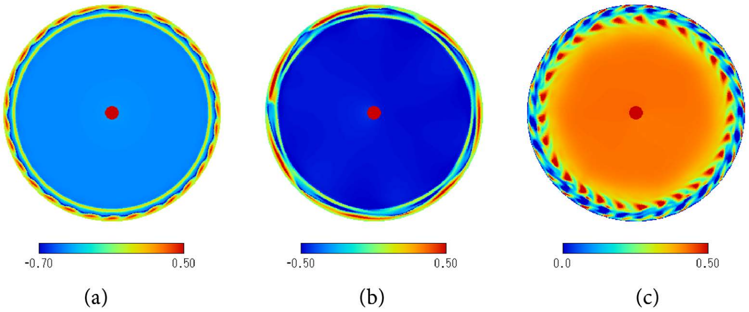

Figure 2. Transition of vortex structures.

5. Visualization Theory and Computational Software

5.1. Second Invariant *Q* of the Velocity Gradient Tensor

In this study, vortex regions in the flow field are indirectly observed by using the fact that regions where the second invariant of the velocity gradient tensor becomes $Q > 0$ correspond to vortex regions. For the velocity gradient tensor D_{ij}, the symmetric component—the strain-rate tensor (deformation tensor) S_{ij}—and the antisymmetric component—the vorticity tensor Ω_{ij}—are defined as follows:

$$D_{ij} = \frac{\partial u_i}{\partial x_j} = S_{ij} + \Omega_{ij} \tag{2}$$

$$S_{ij} = \frac{1}{2}\left(D_{ij} + D_{ji}\right) \tag{3}$$

$$\Omega_{ij} = \frac{1}{2}\left(D_{ij} - D_{ji}\right) \tag{4}$$

The second invariant Q of the velocity gradient tensor is expressed using S_{ij} and Ω_{ij} as:

$$Q = \frac{1}{2}\left(\Omega_{ij}\Omega_{ij} - S_{ij}S_{ij}\right) \tag{5}$$

Furthermore, the velocity gradient tensor can be expanded in cylindrical coordinates (r, θ, z) as:

$$\begin{aligned} Q = &-\frac{1}{2}\left\{\left(\frac{\partial u}{\partial r}\right)^2 + \left(\frac{1}{r}\frac{\partial v}{\partial \theta} + \frac{u}{r}\right)^2 + \left(\frac{\partial w}{\partial z}\right)^2\right\} \\ &-\frac{\partial}{\partial r}\left(\frac{v}{r}\right)\frac{\partial u}{\partial \theta} - \frac{\partial w}{\partial r}\frac{\partial u}{\partial z} - \frac{1}{r}\frac{\partial w}{\partial \theta}\frac{\partial v}{\partial z} \end{aligned} \tag{6}$$

When $Q > 0$ in any region, that region can be interpreted as one where rotation dominates over deformation, and vortex regions can be identified from the distribution of Q.

5.2. Visualization Targets

Visualization was performed using Tecplot 360 EX 2021 R2. For each Reynolds number and disk thickness, x-y cross-section contour plots of Q (iso-value plots) and x-z cross-section plots of Q, radial velocity $\boldsymbol{u}$, and circumferential velocity $\boldsymbol{v}$ (cross-sections of the radial gap) were examined. Fully developed vortices were visualized and compared. The elapsed time used in this study was 100 seconds.

6. Computational Results

For **Figures 3-14**, panel (a) shows the iso-surface of Q at 2 mm above the rotating disk, while panels (b), (c), and (d) show the reference cross-sections of Q, radial velocity u, and circumferential velocity v, respectively. For the same Reynolds number, the range of each parameter is identical across all cases.

6.1. Case of *Re* = 5000

6.1.1. Case of h_d = 10.0 mm, *Re* = 5000

(a) Spiral vortices are observed.

(b) Two disturbed vortices are observed.

(c) Reverse flow is seen near the upper and lower ends of the cylindrical container. In addition, forward flow is observed moving toward the center of the radial gap.

(d) The light-blue region begins to diffuse near the center. Distortions are also observed in the distribution of the green, yellow-green, orange, and red regions.

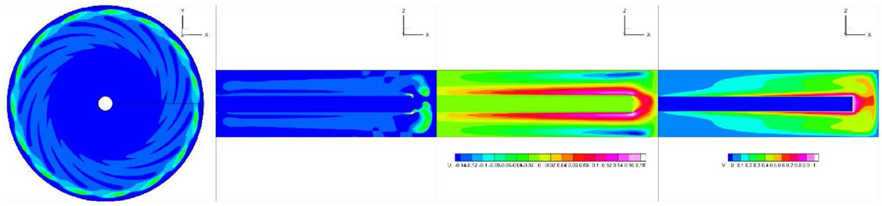

(a) Q (b) u (c) v (d) w

Figure 3. Contour at $h_d = 10.0$ mm, $Re = 5000$.

6.1.2. Case of h_d = 20.0 mm, Re = 5000

(a) Bead vortices are observed.

(b) Multiple disturbed vortices are observed. Compared with 6.2.1, regions of red (high Q values) appear.

(c) Reverse flow is observed near the upper and lower ends of the cylindrical container, as well as in the center of the radial gap.

(d) Although the distribution is streamline-like, disturbances are observed in the yellow-green, orange, and red regions.

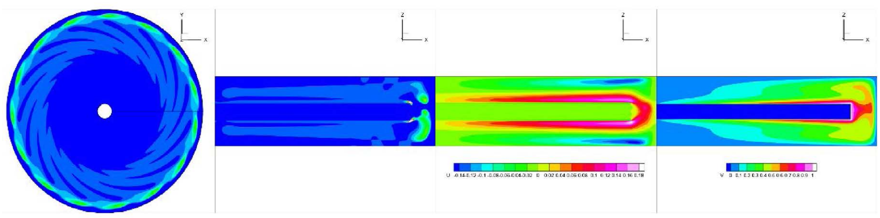

(a) Q (b) u (c) v (d) w

Figure 4. Contour at $h_d = 20.0$ mm, $Re = 5000$.

6.1.3. Case of h_d = 30.0 mm, Re = 5000

(a) Ring vortices are observed.

(b) Two stable vortices are observed.

(c) No significant reverse flow is seen in the radial direction, and forward flow is found to merge toward the center of the radial gap.

(d) Although the distribution is streamline-like, it converges toward the radial gap.

6.2. Case of Re = 10000

6.2.1. Case of h_d = 10.0 mm, Re = 10000

(a) Although the distribution is biased toward low Q values, a swirling pattern is observed, suggesting the presence of spiral vortices.

(b) Multiple underdeveloped vortices are observed.

(c) Reverse flow is seen near the upper and lower ends of the cylindrical container. Forward flow merges toward the center of the radial gap, but disturbances are observed in the forward flow.

(d) Compared with a streamline-like distribution, the circumferential velocity distribution appears to retreat toward the lower radial direction.

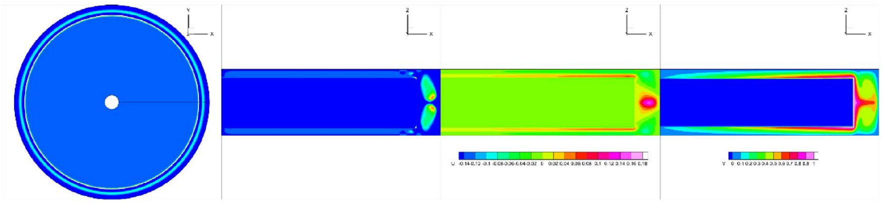

(a) Q (b) u (c) v (d) w

Figure 5. Contour at h_d = 30.0 mm, Re = 5000.

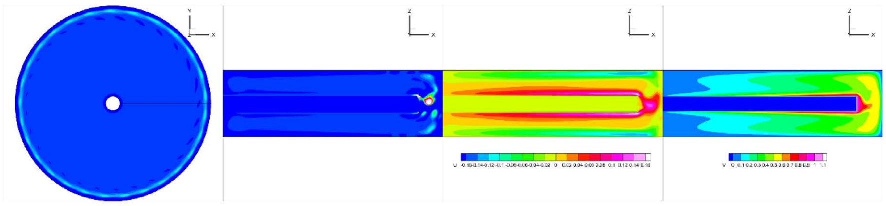

(a) Q (b) u (c) v (d) w

Figure 6. Contour at h_d = 10.0 mm, Re = 10000.

6.2.2. Case of h_d = 20.0 mm, Re = 10000

(a) A vortex structure intermediate between sickle vortices and spiral vortices is observed.

(b) Two disturbed vortices and three underdeveloped vortices are observed.

(c) Reverse flow is observed near the upper and lower ends of the cylindrical container, as well as in the center of the radial gap.

(d) Although the distribution is streamline-like, the orange and red regions exhibit a diffused distribution relative to the radial gap.

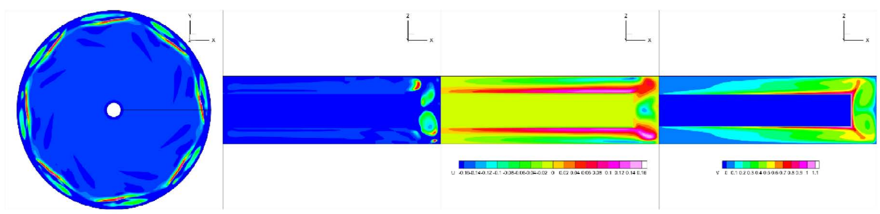

(a) Q (b) u (c) v (d) w

Figure 7. Contour at h_d = 20.0 mm, Re = 10000.

6.2.3. Case of h_d = 30.0 mm, Re = 10000

(a) Bead vortices are observed.

(b) Compared with 6.4.2, two stable vortices and multiple vortices that appear underdeveloped are observed.

(c) Reverse flow is observed near the upper and lower ends of the cylindrical container, as well as in the center of the radial gap.

(d) The distribution is streamline-like. Regions of low velocity exhibit a swirling pattern toward the radial gap, whereas high-velocity regions exhibit a diffused pattern relative to the gap.

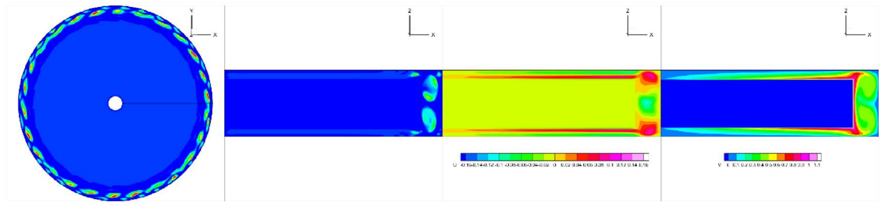

(a) Q (b) u (c) v (d) w

Figure 8. Contour at h_d = 30.0 mm, Re = 10000.

6.3. Case of *Re* = 15000

6.3.1. Case of h_d = 10.0 mm, *Re* = 15000

(a) The vortex structure collapses, suggesting transition to turbulence.

(b) Multiple underdeveloped vortices are observed.

(c) Reverse flow is observed near the upper and lower ends of the cylindrical container. Forward flow merges toward the radial gap, but disturbances are present.

(d) Compared with a streamline-like distribution, the circumferential velocity distribution appears to retreat toward the lower radial direction. Fragmentation of the orange region is also observed.

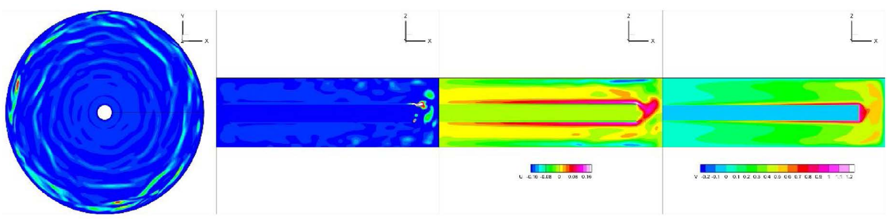

(a) Q (b) u (c) v (d) w

Figure 9. Contour at h_d = 10.0 mm, Re = 15000.

6.3.2. Case of h_d = 20.0 mm, *Re* = 15000

(a) A vortex structure intermediate between sickle vortices and spiral vortices is observed.

(b) Two disturbed vortices and one vortex that appears underdeveloped are observed.

(c) Reverse flow is observed near the upper and lower ends of the cylindrical container, as well as in the center of the radial gap.

(d) Compared with a streamline-like distribution, the circumferential velocity distribution appears to retreat toward the lower radial direction. Orange and red regions exhibit a diffused distribution relative to the radial gap.

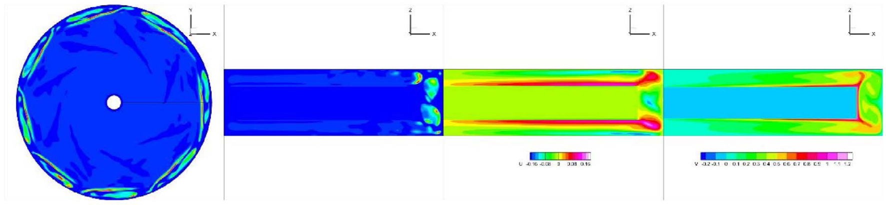

(a) Q (b) u (c) v (d) w

Figure 10. Contour at h_d = 20.0 mm, Re = 15000.

6.3.3. Case of h_d = 30.0 mm, Re = 15000

(a) Spiral vortices are observed.

(b) Disturbed vortex structures and multiple vortices that appear underdeveloped are observed.

(c) Reverse flow is observed near the upper and lower ends of the cylindrical container, as well as in the center of the radial gap.

(d) Although the distribution is streamline-like, the red region appears to stagnate near the edge of the radial gap.

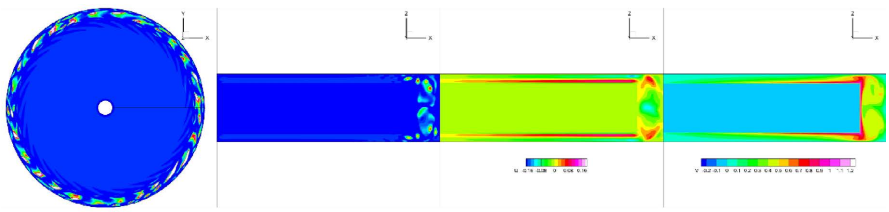

(a) Q (b) u (c) v (d) w

Figure 11. Contour at h_d = 30.0 mm, Re = 15000.

6.4. Case of Re = 20000

6.4.1. Case of h_d = 10.0 mm, Re = 20000

(a) The vortex structure collapses, suggesting transition to turbulence.

(b) Multiple underdeveloped vortices are observed.

(c) Reverse flow is observed near the upper and lower ends of the cylindrical container. Forward flow merges toward the radial gap.

(d) Compared with a streamline-like distribution, the circumferential velocity distribution appears to retreat toward the lower radial direction. Irregularities are observed in the distribution of the orange region.

6.4.2. Case of h_d = 20.0 mm, Re = 20000

(a) A vortex structure intermediate between sickle vortices and spiral vortices, or a sickle vortex transitioning toward turbulence, is observed.

(b) Multiple disturbed vortices and underdeveloped vortices are observed.

(c) Reverse flow is observed near the upper and lower ends of the cylindrical container, as well as in the center of the radial gap.

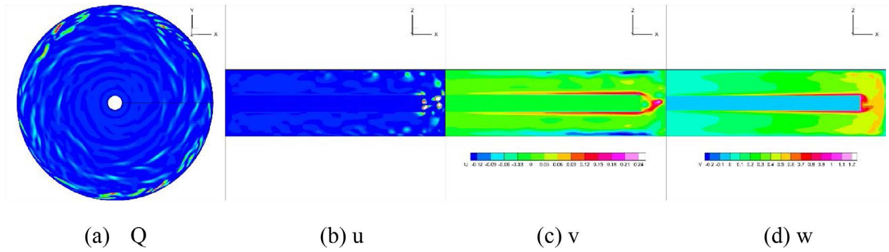

Figure 12. Contour at h_d = 10.0 mm, Re = 20000.

(d) Compared with a streamline-like distribution, the circumferential velocity distribution appears to retreat toward the lower radial direction. Orange and red regions exhibit a diffused pattern relative to the radial gap.

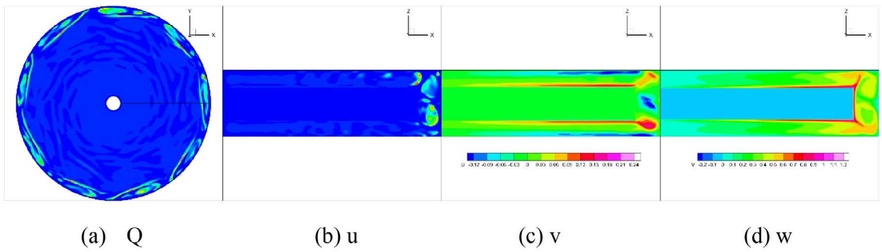

Figure 13. Contour at h_d = 20.0 mm, Re = 20000.

6.4.3. Case of h_d = 30.0 mm, Re = 20000

(a) Spiral vortices are observed.

(b) Multiple underdeveloped vortices are observed.

(c) Reverse flow is observed near the upper and lower ends of the cylindrical container, as well as in the center of the radial gap.

(d) Although the distribution is streamline-like, the orange and red regions exhibit a diffused pattern relative to the radial gap.

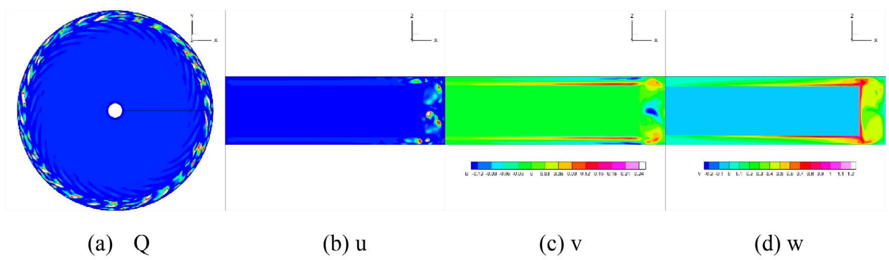

Figure 14. Contour at h_d = 30.0 mm, Re = 20000.

7. Discussion

The results highlight the significant influence of axial gap size on the development and stability of vortex structures around the rotating disk. Based on the results obtained in this study, we interpret the findings as follows. When the axial gap is small, the vertical confinement intensifies the circumferential velocity gradient near the disk surface. This enhanced gradient strengthens the centrifugal force acting on the fluid, which in turn suppresses the reverse-flow components of the radial velocity. As a result, vortex structures tend to remain more laminar-like, even at moderately high Reynolds numbers.

In contrast, larger axial gaps allow the flow to develop more freely in the vertical direction. This additional space reduces the stabilizing effect of the centrifugal force gradient and permits stronger three-dimensional motion. Consequently, vortex structures transition more readily into spiral vortices as the Reynolds number increases.

Interestingly, no clear correlation was observed between the number of vortices and the specific combinations of Reynolds number and disk thickness. This suggests that vortex count is not governed by a single parameter but instead emerges from a complex interplay of shear layers, confinement effects, and inertial forces.

Overall, the findings indicate that axial gap size is a key geometric factor controlling vortex morphology and flow stability in rotating-disk systems. Understanding this relationship provides valuable insight into how disk geometry can be optimized for applications involving high-speed rotation and confined fluid environments.

8. Conclusions

This study numerically investigated the influence of axial gap size on vortex formation around a rotating disk. By varying disk thickness and Reynolds number, the simulations revealed a clear sequence of vortex transitions—from bead vortices to sickle vortices and ultimately to spiral vortices—though not entirely true under all calculation conditions; generally speaking, this sequence held as the flow evolved from laminar to turbulent regimes.

The results demonstrated that axial gap size plays a decisive role in determining vortex morphology. Smaller axial gaps intensify circumferential velocity gradients and suppress vertical flow development, leading to more stable, laminar-like vortex structures even at moderately high Reynolds numbers. In contrast, larger axial gaps allow stronger three-dimensional motion, promoting earlier formation of spiral vortices as inertial effects become dominant.

These findings provide valuable insight into how geometric confinement influences rotating-disk flows. Understanding this relationship can contribute to improved design and optimization of rotating machinery, particularly in applications where flow stability, drag reduction, or vortex control are critical.

Author Contributions

H.F. conceived and designed the study. Y.N. performed the experiments. All authors reviewed and approved the final manuscript.

Funding

This research was conducted with funding from the Nitto Foundation.

Conflicts of Interest

The authors declare no conflicts of interest regarding the publication of this paper.

References

[1] Kármán, T.V. (1921) Über laminare und turbulente Reibung. *Zeitschrift für Angewandte Mathematik und Mechanik*, **1**, 233-252. https://doi.org/10.1002/zamm.19210010401

[2] Bödewadt, U.T. (1940) Die Drehströmung über festem Grunde. *Zeitschrift für Angewandte Mathematik und Mechanik*, **20**, 241-253. https://doi.org/10.1002/zamm.19400200502

[3] Schouveiler, L., Le Gal, P. and Chauve, M.P. (2001) Instabilities of the Flow between a Rotating and a Stationary Disk. *Journal of Fluid Mechanics*, **443**, 329-350. https://doi.org/10.1017/s0022112001005328

[4] Alfredsson, P.H., Kato, K. and Lingwood, R.J. (2024) Flows over Rotating Disks and Cones: A Modern Review. *Annual Review of Fluid Mechanics*, **56**, 45-68. https://doi.org/10.1146/annurev-fluid-121021-043651

[5] Viazzo, S., Poncet, S., Serre, E., Randriamampianina, A. and Bontoux, P. (2012) High-Order Large Eddy Simulations of Confined Rotor-Stator Flows. *Flow, Turbulence and Combustion*, **88**, 63-75. https://doi.org/10.1007/s10494-011-9345-0

[6] Launder, B., Poncet, S. and Serre, E. (2010) Laminar, Transitional, and Turbulent Flows in Rotor-Stator Cavities. *Annual Review of Fluid Mechanics*, **42**, 229-248. https://doi.org/10.1146/annurev-fluid-121108-145514

[7] Lopez, J.M., Marques, F., Rubio, A.M. and Avila, M. (2009) Crossflow Instability of Finite Bödewadt Flows: Transients and Spiral Waves. *Physics of Fluids*, **21**, Article ID: 114107. https://doi.org/10.1063/1.3262817

[8] Cros, A. and Le Gal, P. (2002) Spatiotemporal Intermittency in the Torsional Couette Flow between a Rotating and a Stationary Disk. *Physics of Fluids*, **14**, 3755-3765. https://doi.org/10.1063/1.1508796

[9] Spohn, A., Mory, M. and Hopfinger, E.J. (1998) Experiments on Vortex Breakdown in a Confined Flow Generated by a Rotating Disc. *Journal of Fluid Mechanics*, **370**, 73-99. https://doi.org/10.1017/s0022112098002092